OPEN

Crystallization-aided extraordinary plastic deformation in nanolayered crystalline Cu/amorphous Cu-Zr micropillars

J. Y. Zhang, G. Liu & J. Sun

State Key Laboratory for Mechanical Behavior of Materials, Xi'an Jiaotong University, Xi'an, 710049, P.R. China.

Metallic glasses are lucrative engineering materials owing to their superior mechanical properties such as high strength and great elastic strain. However, the Achilles' heel of metallic amorphous materials — low plasticity caused by instantaneous catastrophic shear banding, significantly undercut their structural applications. Here, the nanolayered crystalline Cu/amorphous Cu-Zr micropillars with equal layer thickness spanning from 20–100 nm are uniaxially compressed and it is found that the Cu/Cu-Zr micropillars exhibit superhigh homogeneous deformation ($\geq$ 30% strain) rather than localized shear banding at room temperature. This extraordinary plasticity is aided by the deformation-induced devitrification via absorption/annihilation of abundant dislocations, triggering the cooperative shearing of shear transformation zones in glassy layers, which simultaneously renders the work-softening. The synthesis of such heterogeneous nanolayered structure not only hampers shear band generation but also provides a viable route to enhance the controllability of plastic deformation in metallic glassy composites via deformation-induced devitrification mechanism.

The widespread enthusiasm for research on metallic glasses (MGs)[1–3] is driven by both a fundamental interest in the structure and properties of disordered and nonequilibrium materials and their unique promise for structural and functional applications, in particular for small-scale applications, such as nano- and micro-electromechanical systems (NEMS and MEMS)[4–6]. Although many bulk MGs exhibit high strength and show substantial fracture toughness, they lack tensile ductility and fail in an apparently brittle manner in unconstrained loading geometries[7]. For instance, some bulk MGs exhibit significant plastic deformation in compression or bending tests, but all exhibit negligible plasticity ($<$ 0.5% strain) in uniaxial tension[1–3]. To overcome brittle failure in tension, introducing an additional crystalline phase into a MG matrix is capable of suppressing such shear failure, resulting in enhanced global plasticity by forming multiple shear bands (SBs) and SB patterns[8–10]. Another effective approach to suppress the catastrophic failure of MGs is synthesizing crystalline/amorphous (C/A) nanolaminates with tensile strength $\sim$ 1–3 GPa and tensile ductility of $\sim$ 3–14% via integrating crystalline and amorphous layers[11,12].

Since MGs are not in thermodynamic equilibrium, supplying such alloys with sufficient energy can promote a phase transformation from an amorphous to a more stable crystalline phase. Mechanical energy in the form of plastic deformation thus can trigger the formation of nanocrystals from the glassy phases, which is well known as deformation-induced devitrification (DID)[13–18]. For monolithic MGs, DID can effectively improve their ductility due to the propagation of SBs can be inhibited by the crystallites[8,17–19], implying the high controllability of the plastic flow of MGs can be achieved. However, the underlying physical mechanism of DID and how this unique phenomenon influences the mechanical behaviors of MGs matrix composites and/or C/A nanolaminates remains shrouded in much mystery. Here, the interplay between the amorphous layers and crystalline layers as well as their mutual effects on mechanical behavior was revealed by investigating the extraordinary plastic deformation in nanolayered crystalline Cu/amorphous Cu-Zr pillars under compression condition at low strain rate and room temperature.

Results

Microstructure of C/A micropillars. The XRD patterns of as-deposited C/A Cu/Cu-Zr multilayers reveal a strong (111) peak in Cu, which broadens with decreasing layer thickness (h). The peak intensity of glassy $Cu_{60}Zr_{40}$
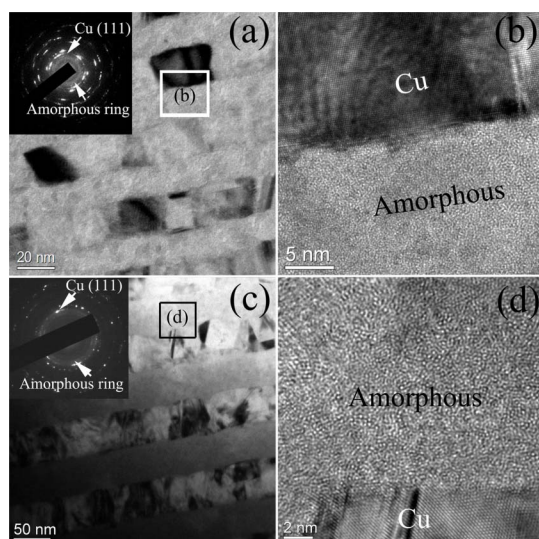
Figure 1 | TEM images of (a) $h = 20$ nm and (c) $h = 50$ nm C/A multilayers. Inset is the corresponding selected area diffraction patterns (SADP), showing strong Cu (111) texture and diffuse amorphous ring. (b) and (d) Magnified view of square region in (a) and (c), respectively, showing amorphous nature of glassy Cu-Zr layer.

is quite low in all of the C/A multilayers, which agrees well with the observed weak amorphous humps in monolithic amorphous films in the diffraction angle range (2θ) of 35–45°. The typical cross-sectional TEM images of $h = 20$ and 50 nm C/A multilayers unveils drastic contrast differences between nanocrystalline Cu and amorphous Cu-Zr layers, as respectively shown in Fig. 1(a) and (c), from which one can clearly see the modulated layered structure as well as internal amorphous structure in glassy Cu-Zr layer. The selected area diffraction pattern (SADP) shown in the inset of Fig. 1(a) and (c) also exhibited a diffuse amorphous ring, as is verified by the HRTEM observations in Fig. 1(b) and (d). In all of the C/A multilayers, the interfaces of C/A multilayers (CAIs) are quite distinguishable, see Fig. 1(b and (d)). Detailed descriptions about the microstructure of multilayers have been described elsewhere[20,21].

Deformation morphologies and mechanical response of C/A micropillars. The typical FIB/SEM images taken before and after uniaxial compression of nanolayered micropillars with $h = 50$ nm were shown in Fig. 2(a) and (b), respectively. It appears that the deformed pillar at strain $\sim$ 20% shows plastic barreling instead of shear banding and extrusion of material from the individual Cu layers, as proved by the point energy analysis[20]. Further cross-sectional FIB/SEM observations revealed that no shear fracture occurred in glassy layers in $\sim$ 20% strained C/A pillars with $h \leq$ 50 nm, even if the maximum strength of C/A pillars ($\sim 2.3 \pm$ 0.1 GPa) sharply overwhelm the yield strength of amorphous $Cu_{60}Zr_{40}$ ($\sim 1.7 \pm 0.05$ GPa), as shown in Fig. 2(c).

The representative true stress-strain curves of the C/A pillars with three different layer thicknesses are shown in Fig. 2(d). It is found that the C/A pillars exhibit smooth plastic flow, supporting the absence of shear banding events often associated with monotonic MGs. This is in sharp contrast with the jerky true stress-strain response of amorphous pillars (see inset in Fig. 2d). Moreover, it is noteworthy that in Fig. 2(d) the maximum strength of C/A pillars monotonically increases from $\sim$ 1.7 $\pm$ 0.05 to 2.3 $\pm$ 0.1 GPa as h decreases from 100 to 20 nm. In other words, the size-driven strength appears to increase in a "smaller is stronger" fashion. Another intriguing feature is that the true stress-strain response of C/A pillar gradually shifts from initial strain hardening (at low plastic strain $\varepsilon_p <$ 10%) to work softening (at high plastic strain $\varepsilon_p >$ 10%).
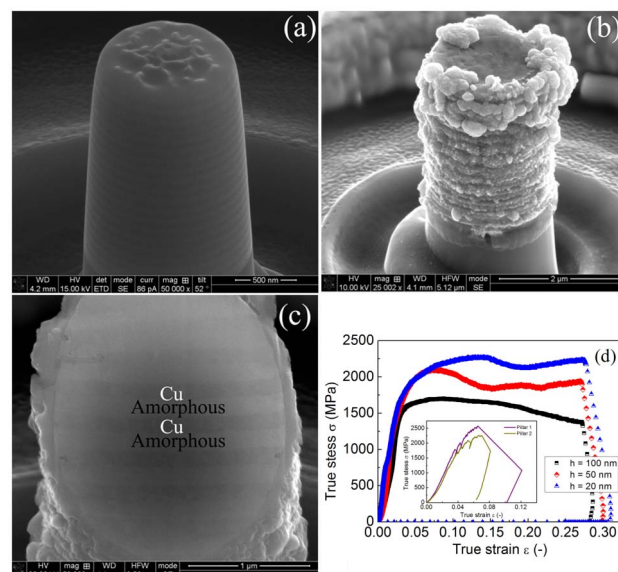

Figure 2 | Typical SEM images of nanolayered Cu/Cu-Zr micropillars with $h = 50$ nm (a) before and (b) after the uniaxial compression tests at $\sim$ 20% strain, show barreling of the micropillar and extrusion of individual Cu layers. (c) The cross-sectional image of the deformed pillar, showing the layered structure and uniformly thinned Cu layers. (d) The true stress - strain plot for Cu/Cu-Zr micropillars with three different layer thicknesses showing strain hardening-to-softening transition. Inset is the true stress – strain curves of amorphous pillars associated with shear banding induced-strain burst.

In particular, the $h = 100$ nm pillars exhibit weak even no strain hardening, while the smaller h pillars present stronger hardening behavior. The increased strain hardening capability with reducing h is caused by more glide dislocation-interface interactions[20,22,23]. In contrast, there is a propensity that smaller h pillars exhibit more pronounced softening behavior owing to more CAIs acting as dislocation sinks exist in the smaller h pillars[12,20].

Internal structure features of compressed C/A micropillars. To further explore the nanoscaled mechanical properties of the as-deposited C/A multilayers and unveil the underlying physical mechanisms of their extraordinary plasticity, TEM samples were fabricated by FIB from the 30% deformed C/A pillars to observe the detailed deformation features, using a trenching and lift-out technique. Fig. 3(a) is the typical cross-sectional FIB/SEM images of the 30% deformed $h = 50$ nm C/A pillars, from which one can see the wavy CAIs, non-uniform reduction in layer thickness and broken amorphous layers, radically different from the homogeneity in deformation in the 20% compressed C/A pillars. This means that the heterogeneity in the layer thickness reduction and the fragmentation of amorphous layer is only apparent under such severe deformation ($\sim$30% strain). Further TEM observations and EDX analysis of the deformed C/A pillars through-thickness cross-sections are shown in Fig. 3(b–d). We summarize our observations based on TEM observations and EDX analysis as follows: (i) In spite of the non-uniform thickness reduction, there was no interfacial delamination, implying good strain compatibility of CAIs. (ii) There were no traces of fracture or microcracks in nanocrystalline Cu and amorphous Cu-Zr layers, indicating extraordinary homogeneous flow in glassy layers and high compressive deformability of nanolayered Cu/Cu-Zr pillars ($>$ 30% strain) can be achieved without sacrificing strength. (iii) Neither heavy dislocations storage nor abundant planar defects such as stacking faults and deformation twins in the crystalline Cu (and crystalline Cu-Zr phase) layers were observed (see Fig. 3b), implying the nucleated dislocations can be
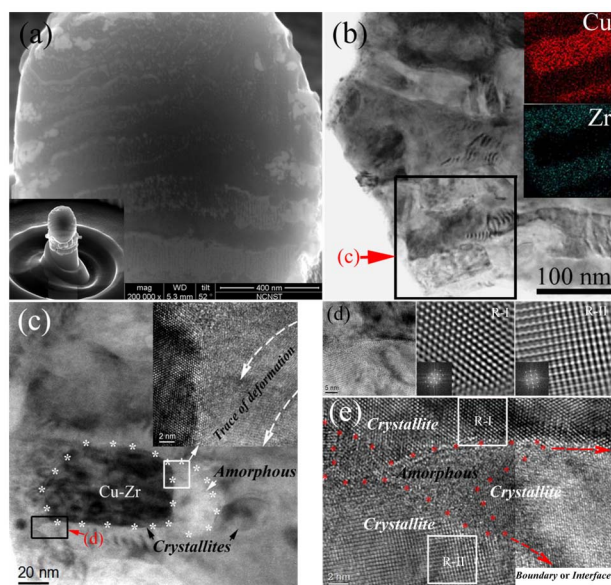
2

Figure 3 | (a) Magnified cross-sectional SEM/FIB image of ~ 30% compressed Cu/Cu-Zr micropillar (see the inset) with $h = 50$ nm, showing wavelike interfaces and broken amorphous layers. Inset is FIB-ed deformed micropillar, showing barreling and extrusion of Cu layers. (b) STEM image and superimposed compositional mapping analysis, demonstrating a chemically alternating layer structure of the deformed micropillars and showing deformation heterogeneity. (c) Magnified TEM image of square white box in (b). Inset is the magnified view of square white box in (c) showing the crystalline phase with scattered lattice fringes as the trace of deformation in amorphous layer. (d) Magnified TEM view of rectangle black area in (c). (e) HRTEM image of (d), showing localized residual amorphous. Insets is respectively the inverse fast Fourier transform (FFT) HRTEM image of region-I (R-I) and region-II (R-II, $Cu_{10}Zr_7$) and the corresponding FFT, showing different crystalline orientations. GBs or interfaces are marked by the asterisks.

absorbed by the opposite CAIs and/or glassy layers. (iv) The amorphous Cu-Zr layers were almost fully crystallized (localized residual amorphous phase can still be found at the junction of grain boundaries (GBs) and CAIs, see Fig. 3c and d). This renders the nanosized crystallites with a wide size range of ~ 10–50 nm rather than the SBs in the glassy layers were frequently observed, suggesting the DID could occur during plastic deformation. (v) The deformation-induced nanophase is orthorhombic $Cu_{10}Zr_7$ phase because the chemical composition of amorphous $Cu_{60}Zr_{40}$ is quite close to that of $Cu_{10}Zr_7$, indicating a possible structural affinity of the $Cu_{10}Zr_7$ phase and the glass on a short range order length scale[24].

Discussion

The extrusion of soft/ductile Cu and absence of SBs in all the deformed C/A pillars suggested that the plastic strain was mainly carried out by the deformation of Cu layers and the full suppression of instantaneous catastrophic shear banding. The underlying reason for the homogeneous-like deformation of the whole C/A pillars under uniaxial compression has been discussed in our previous work[20] in term of the strength discrepancy between the two constituent crystalline and amorphous layers at different length scales. In small length-scale ($10 < h < 60$ nm), the crystalline layer strength and the SB propagation stress are comparable, the propagation of SBs will be effectively suppressed, even if they can form[20]. While in large length-scale ($h > 60$ nm), the maximum strength of C/A pillars will be less than the yield strength of the amorphous phase[20]. No yielding in the amorphous phase implies that there is no possibility to form SBs, and no speaking of propagation of SBs. Under isostress

compression condition, the amorphous layers and crystalline layers are respectively subjected to tensile and compressive stress, resulting in the preferential extension along the lateral direction for the softer Cu layers[20,25]. This consists with the fact that the yield strength of pure amorphous $Cu_{60}Zr_{40} \sim 1.7$ GPa (see the inset in Fig. 2d) is far greater than that of nanocrystalline Cu ~ 1.2 GPa[25], as is the case of $h = 100$ nm C/A pillars. Recent atomic simulations[12,26] revealed that the CAI has random structural variations because of the amorphous phase, leading to interfacial regions with weak shear strengths that are susceptible to sliding (similar to GB sliding) and showing unique inelastic shear (slip) characteristics, as is consistent with the TEM observations[27]. Specifically, the "extreme incompatibility" often emerging at the GBs in crystalline materials, hardly arises at the CAIs, because the shear transformation zones (STZ) in the glassy materials are omnidirectional; e.g., there are infinite selections of possible inelastic shear modes to transfer to[12].

In contrast, at smaller h, the defects in the glass structure (and their groups) become smaller in size and less in population, so that SB initiation becomes a critical issue. Shear banding thus becomes "nucleation controlled" at the outset of its formation[28]. Upon loading, the shear transformations that carry plastic events in MGs will initially operate stochastically, independent of each other from fertile sites (i.e., STZs) in the glassy structure, but they gradually gain correlation both temporally and spatially, and self-organize into a larger and larger flow zone[29]. However, the C/A architecture renders the propagation of SB can be suppressed by strong nanocrystalline layer, since the SB propagation stress is comparable with the crystalline layer strength[20]. Shear banding becomes so unfavorable in the nanolayered materials that it subsides altogether and gives way to STZ operations everywhere, to plastically flow the sample in a "homogeneous-like" fashion[28]. Therefore, homogeneous plasticity is achieved in present nanoscaled amorphous layers instead of instantaneous catastrophic shear failure[11,12,20,30], especially under the confinements imposed in the uniaxial compression test mode.

Judging from the lack of line and planar defects in the crystalline phase and the emergence of crystals in glassy layers, we postulate that the absorption of dislocations nucleated from crystalline phase by glassy layers contributes to DID, which renders the extraordinary plasticity, apart from the intrinsically low stability of the binary Cu-Zr MGs. It is the DID rather than any other mechanism such as the formation of multiple SBs, that renders the extraordinary plasticity here. Although the formation of nanocrystallites is apparently associated with localized shearing flow, the questions natural arise are why DID occurs under high compressive strain at room temperature, and why the amorphous layers are almost fully crystallized at nanoscale (~20–100 nm). It has been reported that both the mass transportation and the temperature rise within SBs and their vicinity produced by significant plastic flow can cause nanocrystallization in the narrow SBs[16,17,31,32]. However, the fact that crystalline CuZr phase almost has the same composition as the parent glass suggests that there is no significant mass transportation occurred during plastic deformation. Moreover, the microcompression tests were performed at ambient temperature far below the glass transition points of amorphous $Cu_{60}Zr_{40}$ and the deformation volume is largely confined, which minimizes the temperature rise contributing to DID. In particular, there is no shear banding occurred avoided directly the consequence of the inevitable dynamic flow dilatation in the actively deforming bands (without any substantial increase in temperature during plastic flow) and of the attendant dramatic enhancement in atomic diffusional mobility[16]. Therefore, we can exclude that the precipitation of the $Cu_{10}Zr_7$ nanocrystals during deformation originates from a temperature rise as well as mass transportation. Instead, we believe that stable plastic flow of the material leads to atomic displacements or arrangements, which directly results in crystallization.

To understand the underlying mechanism of DID, we follow the footsteps of Lu[33] and Lee et al[18] in light of the viewpoints of

thermodynamics and kinetics associated with two different stress states imposed on the samples, i.e., hydrostatic compression and shear. When the uniaxial compression of $\sim$ 2 GPa (corresponding to the maximum strength of present C/A samples) is applied to the sample, it is decomposed into hydrostatic compression ($\sim$1 GPa) and shear stress ($\sim$1 GPa) at the maximum shear plane[18]. The hydrostatic compressive stress can reduce the energy barrier for nucleation; while the shear stress can lower the energy barrier for diffusion and induce the atoms to migrate along the shearing direction, promoting an increase in the local free volume associated with atomic dilatation[18,24]. Analogous to the single-atom squeezing in Spaepen's model[34], the local shear transformations, or the motion of STZs, around free-volume sites can lead to the pushing apart of surrounding atoms along activation paths, resulting in an activation dilatation and thereby lowering the local viscosity and energy barrier for atomic diffusion in localized regions[18,19,24]. Therefore, the simultaneous action of hydrostatic compression and shear stress via uniaxial compression induces an enhancement of the nucleation rate, which promotes crystallization to accommodate the external compressive stress by reducing the volume of the amorphous phase through crystallization at room temperature.

Based on HRTEM observations of the deformed sample in Fig. 3, the nanocrystallites formed during deformation is orthorhombic $Cu_{10}Zr_7$ phase. In this DID process the independent STZs which begin as small regions where the local atomic structure is capable of inelastic rearrangements under an applied stress, could take an important role as the nuclei for the nanocrystallization[17,35]. The STZ-mediated activities, namely cooperative shearing of unstable STZs activated by shear stresses, are the underlying reason to achieve the homogeneous-like flow as well as the amorphous-to-crystalline transition in Cu-Zr layers[36,37]. The cooperative shearing model of STZs[36] correlated the structure of MGs with their energetics by introducing the concept of potential-energy landscape (PEL) in combination with STZs and thus allows one to interpret their deformation that intrinsically depends on the actual size or volumes of STZs[36,37]. As the same fundamental processes are required for plastic flow as for crystallization of amorphous, namely atomic rearrangements, we qualitatively explain the mechanisms underlying the precipitation of orthorhombic $Cu_{10}Zr_7$ nanocrystals on deformation follow the spirit of cooperative shearing model. Viscosity, η, can be expressed as[38]

$$\eta = \eta_0 \exp\left[\frac{\Delta F(T)}{k_B T}\right], \qquad (1)$$

where the pre-exponential constant η_0 is the viscosity at infinite temperature, $\Delta F(T)$ is the temperature-dependent activation energy, k_B is the Boltzmann constant and T is the temperature. The potential energy can be expressed by a sinusoidal function similar to the function used to describe the theoretical shear strength of crystalline solids[38]

$$\frac{Q}{Q_0} = \sin^2\left(\frac{\pi\gamma}{4\gamma_c}\right), \qquad (2)$$

where Q is the potential energy, Q_0 is the amplitude of the energy function, γ is the shear strain and γ_c is a critical shear strain limit. The second derivative of the potential energy with respect to the shear coordinate (representing the curvature of the potential energy function at $\gamma = 0$) gives the instantaneous shear modulus G:

$$\frac{d^2Q}{d\gamma^2}\bigg|_{\gamma=0} = G = \left(\frac{\pi^2}{8\gamma_c^2}\right)Q_0. \qquad (3)$$

The cooperative shearing model assumes that the total barrier height, which has to be surmounted to initiate structural rearrangements, $\Delta F(T)$, is the product of the amplitude of the potential energy function, Q_0, and the size of the cooperatively rearranging zone:

$$\Delta F(T) \equiv Q_0 \Omega = \frac{8\gamma_c^2}{\pi^2} G\Omega. \qquad (4)$$

Eq. (4) links the barrier height with the shear modulus, G, and the size of the rearranging zone, Ω, and provides the basis for the following discussion. It signifies that the barrier separating local minima, $\Delta F(T)$, decreases if the shear modulus decreases or if the size of the rearranging zone is still small and consequently flow is facilitated. When mechanical energy (shear stresses) is introduced into the system, shearing has been found to flatten out the less stable local minima in the PEL (inherent states) and eventually to let them vanish completely, which is equivalent to a significant local softening of G[39,40]. In other words, mechanical loading stimulates structural rearrangements by facilitating flow. The more liquid-like, softened regions in the glass have a higher fragility and are less resistant against crystallization[41]. Without the assistance of long-range atomic diffusion in strained regions, the precipitation of stable equilibrium phases $Cu_{10}Zr_7$ also indicates a possible structural affinity of the $Cu_{10}Zr_7$ phase and the matrix glass on a short range order length scale and the DID process is kinetically favored.

The formation of $Cu_{10}Zr_7$ nanocrystals consumes energy and the growth of these crystals is expected to become more difficult for the larger sized crystals. This follows from Eq. (4), which states that the activation energy of flow is proportional to the size of the rearranging zone, Ω. With deformation proceeded or more energies is introduced into the system, the crystalline nuclei grow up/deform. In any case the precipitation of $Cu_{10}Zr_7$ nanocrystals and their subsequent growth/deformation are expected to have a strong effect on the deformation behavior of the residual glassy matrix. Since the volume of the crystalline phase is normally smaller than that of the amorphous phase, the crystalline nuclei in the amorphous matrix are under internal tension. Therefore, the application of external compression to the specimen relieves the tensile stress endured by the crystalline nuclei and, therefore, stabilizes the crystalline nuclei (i.e. STZs)[18,24]. Johnson and Samwer[36] pointed out that an average shear strain limit of $\sim$ 0.027, or the elastic strain required for the formation of a SB nucleus in bulk MGs that consists of a local collection of STZs, is shared by a population of bulk MGs for plastic yielding. In the light of this, the smaller these collective flow defects (e.g. small aspect ratio of the STZ percolation/collection), the lower the stress concentration, and the lower the possibility for them to reach the threshold that would trigger the self-sustaining shear banding. Thus, STZs with a large size reinforce the shear capability of the metallic glass and promote the formation of multiple SBs, which is consistent with the fact that a higher Poisson's ratio represents a higher possibility for the material to shear under applied stress[37,42]. In addition, the high density of deformation-induced nanocrystals limits SBs propagation and effectively prevents the shear softening by a "self-locking" effect, leading to large plasticity[17].

Next, we will illustrate the underlying reasons for the lack of residual defects (such as dislocations, stacking faults and deformation twins) and mainly focus on the mechanism of atomic arrangements in the DID behavior from the following atom-scale viewpoint. Most recently, Arman $et\ al.$[26] performed large-scale molecular dynamics simulations to investigate plasticity in Cu/$Cu_{46}Zr_{54}$ glass nanolaminates under uniaxial compression. It is revealed that (leading and trailing) partials/full dislocations are observed in the Cu layers and screw dislocations are seen near the CAIs. Further experimental observations and simulations demonstrate that the nanoscale amorphous layer (or the CAI) not only exhibits an extraordinary capacity to act as dislocation sources/sinks but also as effective barrier for dislocations, and do interact with dislocations (including interface-induced screw dislocations), enabling absorption of free volume and free energy transported by the dislocations through CAIs[12,26]. When the incoming dislocations transmit cross the CAI and propagate inside the Cu layer, they will be absorbed by the

opposite CAI (into amorphous layer), leaving no dislocation debris[43,44]. Specifically, the emissions of the trailing partials effectively erase the stacking faults created by the leading partial, which lowers the density of stacking faults in crystalline layers and evidences a lack of abundant defects[45]. Recently, Wang and coworkers[12] pointed out that the glassy layers can significantly impact dislocation structures formed in the nanocrystalline layers via the attraction and annihilation of dislocations in the amorphous layers. It can dramatically decrease dislocation density in the nanocrystalline layers causing work-softening at high strains as observed in the true stress-strain curves. Concomitantly, the absorbed dislocations would stimulate atomic arrangements triggering the DID process. This is because that as the nucleated partial/full dislocations (from the CAIs or GBs or free surface or CAI-GB interaction) impinges on or moves along CAIs, they will activate STZs in a correlated fashion near the intersection line between the dislocation slip plane and ACI without significant atomic rearrangements in its surrounding glassy matrix[12,26]. They subsequently trigger other STZs nearby, and the entire inelastically deformed zone "diffuses" gradually into the deeper amorphous region[12]. Because the activations of individual STZs in an embryonic SB are independent of each other under applied stresses at room temperature[37,46], interactions between these activation units of plastic flow in the bulk MGs are thus unlikely to alter the mechanism of plastic flow in the consecutive deformation of MGs. During the DID process, these crystalline nuclei gradually grow up through transforming glass matrix into nanocrystallites by continuously trapping dislocations[17,35]. Meanwhile, the abundant dislocations absorbed by glassy layers can provide partial energy for the amorphous-to-crystalline transformation as well as the growth of crystalline embryos, in addition to the mechanical energy (external stress).

The attainment of both strength and ductility is a vital requirement for most structural materials. We showed the attainment of superior strength beyond $\sim$ 2.0 GPa and great deformability over $\sim$ 30% in nanolayered crystalline Cu/amorphous $Cu_{60}Zr_{40}$ micropillars and uncovered the DID in crystalline Cu/amorphous $Cu_{60}Zr_{40}$ multilayers and almost defects free in deformed nanocrystals. This crystallization mechanism stem from the combination of dislocations-stimulated-STZs activities first and collections of STZ-trapping dislocations afterwards in glassy layers. It provides a viable way to counterbalance shear banding-induced softening generally witnessed in bulk MGs and can effectively enhance their controllability of plastic deformation. The concept of DID-aided superior deformability via "external-supplied" dislocations-stimulated-STZs probably opens a new and universal strategy to synthesize self-toughening bulk MGs, which deals with the Valiev's "paradoxon" of structural materials, especially of the MG matrix composites.

Methods

Multilayer synthesis and microstructure characterization. The $\sim$ 2 μm-thick Cu/Cu-Zr C/A multilayers with equal layer thickness (h) varying from 20 to 100 nm and monotonic $Cu_{60}Zr_{40}$ amorphous films were deposited on Si (100) substrates by direct current (DC) magnetron sputtering at room temperature. Cu (99.995%) and Zr (99.99%) targets were used to produce alternating layers of nanocrystalline pure Cu and amorphous $Cu_{60}Zr_{40}$ (atomic fraction). The internal structure features of as-deposited Cu/Cu-Zr and $Cu_{60}Zr_{40}$ films was characterized by X-ray diffraction and transmission electron microscopy (TEM). High resolution transmission electron microscopy (HR-TEM) and energy dispersive X-ray (EDX) analyses to identify the elemental composition and the interface integrity of the specimens were performed on an JEOL-2100F TEM, with Fischione a ultra-high resolution high-angle annular dark field detector (0.23 nm resolution in STEM image mode) and Oxford instruments EDX detector with a spatial resolution of $\sim$ 1 nm for chemical analysis. Detailed descriptions about the preparation of multilayers have been described elsewhere[21].

Flat punch compression test of nanolayered micropillars. To further explore their micro-scaled mechanical properties, the small tapered ($\sim$2–4°) nanolayered Cu/Cu-Zr micropillars with diameter (ϕ)$\sim$ 950 nm were fabricated from the as-deposited multilayers using a Helios Nano Lab 600i dual-beam focused ion beam (FIB) system, which also allows scanning electron microscopy (SEM) imaging. To minimize the

potential damage from ion irradiation due to the Ga ion beam and to clean any newly-deposited materials from the pillar surface, the final FIB fine milling step was performed under a lowered voltage (15 kV) and current (15 pA). For comparison reasons, the ϕ = 950 nm $Cu_{60}Zr_{40}$ amorphous pillars were also prepared and then compressed at the same condition as mentioned above.

All the pillars were then uniaxially compressed in a Hystron Ti 950 with a 10 μm side-flat quadrilateral cross-section diamond indenter at constant strain rate of 2 $\times$ 10^{-4} s^{-1} up to $\sim$ 20–30% strain. Force-displacement data were continuously recorded, and the initial geometry of the pillar was measured from the SEM images. True stress-strain curves were calculated using a constant volume and homogeneous deformation assumption model to characterize the deformation behaviors[47,48]. Because of the amount of time required to conduct the vast majority of compression experiments, considerable efforts have been devoted to correcting for thermal drift to improve the reliability and accuracy of the present nanoscale deformation measurements. In the present work, the allowable-drift-rate was set at 0.005 nm s^{-1}, which is 20-times smaller than the typical value (0.1 nm s^{-1}) used in the testing of films/micropillars such that the effect of thermal drift could be minimized and neglected. More details about the micropillars preparation procedures, testing methods and true stress-strain curve calculation procedure can be found in Ref.[20].

1. Wang, W. H. The elastic properties, elastic models and elastic perspectives of metallic glasses. *Progress in Materials Science* **57**, 487–656 (2012).
2. Cheng, Y. Q. & Ma, E. Atomic-level structure and structure–property relationship in metallic glasses. *Progress in Materials Science* **56**, 379–473 (2011).
3. Trexler, M. M. & Thadhani, N. N. Mechanical properties of bulk metallic glasses. *Progress in Materials Science* **55**, 759–839 (2010).
4. Ashby, M. F. & Greer, A. L. Metallic glasses as structural materials. *Scripta Materialia* **54**, 321–326 (2006).
5. Greer, A. L. Metallic glasses. *Science* **267**, 1947–1953 (1995).
6. Demetriou, M. A damage-tolerant glass. *Nature Mater.* **10**, 123–128 (2011).
7. Schuh, C. A., Hufnagel, T. C. & Ramamurty, U. Mechanical behavior of amorphous alloys. *Acta Materialia* **55**, 4067–4109 (2007).
8. Das, J. *et al.* 'Work-hardenable' ductile bulk metallic glass. *Physical Review Letters* **94**, 205501 (2005).
9. Hofmann, D. C. *et al.* Designing metallic glass matrix composites with high toughness and tensile ductility. *Nature* **451**, 1085–1089 (2008).
10. Hays, C. C., Kim, C. P. & Johnson, W. L. Microstructure controlled shear band pattern formation and enhanced plasticity of bulk metallic glasses containing in situ formed ductile phase dendrite dispersions. *Physical Review Letters* **84**, 2901–2904 (2000).
11. Kim, J. Y., Jang, D. C. & Greer, J. R. Nanolaminates Utilizing Size-Dependent Homogeneous Plasticity of Metallic Glasses. *Advanced Functional Materials* **21**, 4550–4554 (2011).
12. Wang, Y. M., Li, J., Hamza, A. V. & Barbee, J. T. W. Ductile crystalline-amorphous nanolaminates. *Proceedings of the National Academy of Sciences of the United States of America* **104**, 11155–11160 (2007).
13. He, Y., Shiflet, G. J. & Poon, S. J. Ball milling-induced nanocrystal formation in aluminum-based metallic glasses. *Acta Metallurgica et Materialia* **43**, 83–91 (1995).
14. Guo, F. Q. & Lu, K. Formation of a single α-Fe nanophase during mechanically driven crystallization of an FeMoSiB metallic glass. *Nanostructured Materials* **7**, 509–517 (1996).
15. Wang, K. *et al.* Micromechanisms of serrated flow in a Ni50Pd30P20 bulk metallic glass with a large compression plasticity. *Acta Materialia* **56**, 2834–2842 (2008).
16. Kim, J. J., Choi, Y., Suresh, S. & Argon, A. S. Nanocrystallization During Nanoindentation of a Bulk Amorphous Metal Alloy at Room Temperature. *Science* **295**, 654 (2002).
17. Chen, M. Extraordinary plasticity of ductile bulk metallic glasses. *Physical Review Letters* **96**, 245502 (2006).
18. Lee, S. W., Huh, M. Y., Fleury, E. & Lee, J. C. Crystallization-induced plasticity of Cu–Zr containing bulk amorphous alloys. *Acta Materialia* **54**, 349–355 (2006).
19. Chen, M. Mechanical Behavior of Metallic Glasses: Microscopic Understanding of Strength and Ductility. *Annu Rev Mater Res* **38**, 445–469 (2008).
20. Zhang, J. Y., Liu, G., Lei, S. Y., Niu, J. J. & Sun, J. Transition from homogeneous-like to shear-band deformation in nanolayered crystalline Cu/amorphous Cu–Zr micropillars: Intrinsic vs. extrinsic size effect. *Acta Materialia* **60**, 7183–7196 (2012).
21. Zhang, J. Y. *et al.* Mechanical properties of crystalline Cu/Zr and crystal–amorphous Cu/Cu–Zr multilayers. *Materials Science and Engineering: A* **552**, 392–398 (2012).
22. Zhang, J. Y. *et al.* Length scale-dependent deformation behavior of nanolayered Cu/Zr micropillars. *Acta Materialia* **60**, 1610–1622 (2012).
23. Zhang, J. Y. *et al.* Intrinsic and extrinsic size effects on deformation in nanolayered Cu/Zr micropillars: From bulk-like to small-volume materials behavior. *Acta Materialia* **60**, 4054–4064 (2012).
24. Lee, S. W., Huh, M. Y., Chae, S. W. & Lee, J. C. Mechanism of the deformation-induced nanocrystallization in a Cu-based bulk amorphous alloy under uniaxial compression. *Scripta Materailia* **54**, 1439–1444 (2006).
25. Liu, M. C., Lee, C. J., Lai, Y. H. & Huang, J. C. Microscale deformation behavior of amorphous/nanocrystalline multilayered pillars. *Thin Solid Films* **518**, 7295–7299 (2010).

26. Arman, B. *et al.* Plasticity in Cu(111)/Cu46Zr54 glass nanolaminates under uniaxial compression. *Journal of Applied Physics* **110**, 043539 (2011).

27. Gao, H., Zhang, L. & Baker, S. P. Dislocation core spreading at interfaces between metal films and amorphous substrates. *Journal of the Mechanics and Physics of Solids* **50**, 2169–2202 (2002).

28. Wang, C. C. *et al.* Sample size matters for Al88Fe7Gd5 metallic glass: Smaller is stronger. *Acta Materialia* **60**, 5370–5379 (2012).

29. Falk, M. L. & Langer, J. S. Dynamics of viscoplastic deformation in amorphous solids. *Physical Review E* **57**, 7192–7205 (1998).

30. Jang, D. & Greer, J. R. Transition from a strong-yet-brittle to a stronger-and-ductile state by size reduction of metallic glasses. *Nature Materials* **9**, 215–219 (2010).

31. Chen, H., He, Y., Shiflet, G. & Poon, S. Deformation-induced nanocrystal formation in shear bands of amorphous alloys. *Nature* **367**, 541–543 (1994).

32. Lewandowski, J. J. & Greer, A. L. Temperature rise at shear bands in metallic glasses. *Nature Mater.* **5**, 15–18 (2006).

33. Lu, K. Nanocrystalline metals crystallized from amorphous solids: nanocrystallization, structure, and properties. *Materials Science and Engineering: R: Reports* **16**, 161–221 (1996).

34. Spaepen, F. A microscopic mechanism for steady state inhomogeneous flow in metallic glasses. *Acta Metallurgica* **25**, 407–415 (1977).

35. Hebert, R. J., Perepezko, J. H., Rösner, H. & Wilde, G. Dislocation formation during deformation-induced synthesis of nanocrystals in amorphous and partially crystalline amorphous Al88Y7Fe5 alloy. *Scripta Materialia* **54**, 25–29 (2006).

36. Johnson, W. L. & Samwer, K. A universal criterion for plastic yielding of metallic glasses with a (T/Tg)2/3 temperature dependence. *Physical Review Letter* **95**, 195501 (2005).

37. Pan, D., Inoue, A., Sakurai, T. & Chen, M. W. Experimental characterization of shear transformation zones for plastic flow of bulk metallic glasses. *Proceedings of the National Academy of Sciences of the United States of America* **105**, 14769–14772 (2008).

38. Johnson, W. L., Demetriou, M. D., Harmon, J. S., Lind, M. L. & Samwer, K. Rheology and ultrasonic properties of metallic glass-forming liquids: A potential energy landscape perspective. *MRS Bulletin* **32**, 644–650 (2007).

39. Mayr, S. G. Activation Energy of Shear Transformation Zones: A Key for Understanding Rheology of Glasses and Liquids. *Physical Review Letters* **97**, 195501 (2006).

40. Pauly, S., Gorantla, S., Wang, G., Kühn, U. & Eckert, J. Transformation-mediated ductility in CuZr-based bulk metallic glasses. *Nature Materials* **9**, 473–477 (2010).

41. Ichitsubo, T. *et al.* Microstructure of Fragile Metallic Glasses Inferred from Ultrasound-Accelerated Crystallization in Pd-Based Metallic Glasses. *Physical Review Letters* **95**, 245501 (2005).

42. Schroers, J. & Johnson, W. L. Ductile bulk metallic glasses. *Physical Review Letters* **93**, 255506 (2004).

43. Budrovic, Z., Van Swygenhoven, H., Derlet, P. M., Van Petegem, S. & Schmitt, B. Plastic Deformation with Reversible Peak Broadening in Nanocrystalline Nickel. *Science* **304**, 273–276 (2004).

44. Yamakov, V., Wolf, D., Phillpot, S. R., Mukherjee, A. K. & Gleiter, H. Deformation-mechanism map for nanocrystalline metals by molecular-dynamics simulation. *Nature Materials* **3**, 43–47 (2004).

45. Zhu, Y. T., Liao, X. Z. & Wu, X. L. Deformation twinning in nanocrystalline materials. *Progress in Materials Science* **57**, 1–62 (2012).

46. Schuh, C. A., Lund, A. C. & Nieh, T. G. New regime of homogeneous flow in the deformation map of metallic glasses: Elevated temperature nanoindentation experiments and mechanistic modeling. *Acta Materialia* **52**, 5879–5891 (2004).

47. Greer, J. R., Oliver, W. C. & Nix, W. D. Size dependence of mechanical properties of gold at the micron scale in the absence of strain gradients. *Acta Materialia* **53**, 1821–1830 (2005).

48. Bharathula, A., Lee, S. W., Wright, W. J. & Flores, K. M. Compression testing of metallic glass at small length scales: Effects on deformation mode and stability. *Acta Materialia* **58**, 5789–5796 (2010).

Acknowledgements

Author contributions

J.S. designed the project and guided the research. J.Y.Z. carried out the experiments and proposed the concept. J.Y.Z. and G.L. wrote the paper. All authors contributed to the discussions.

Additional information

Competing financial interests: The authors declare no competing financial interests.

How to cite this article: Zhang, J.Y., Liu, G. & Sun, J. Crystallization-aided extraordinary plastic deformation in nanolayered crystalline Cu/amorphous Cu-Zr micropillars. *Sci. Rep.* **3**, 2324; DOI:10.1038/srep02324 (2013).